Terr. Atmos. Ocean. Sci., Vol. 26, No. 2, Part I, 83-94, April 2015 doi: 10.3319/TAO.2014.09.09.01(T)

Morlet Wavelet Analysis of $M_L \geq 3$ Earthquakes in the Taipei Metropolitan Area

Kou-Cheng Chen[1, *], Jeen-Hwa Wang[1], Kwang-Hee Kim[2], Win-Gee Huang[1], Kao-Hao Chang[1, 3], Jeng-Cheng Wang[4], and Pei-Ling Leu[5]

[1] *Institute of Earth Sciences, Academia Sinica, Taipei, Taiwan, R.O.C.*
[2] *Department of Geological Sciences, Pusan National University, Korea*
[3] *Department of Civil Engineering, Chung Yuan Christian University, Taoyuan, Taiwan, R.O.C.*
[4] *Department of Applied Geoinformatics, Chia Nan University of Pharmacy and Science, Tainan City, Taiwan, R.O.C.*
[5] *Seismological Center, Central Weather Bureau, Taipei, Taiwan, R.O.C.*

Received 13 June 2014, revised 5 September 2014, accepted 9 September 2014

ABSTRACT

$M_L \geq 3$ earthquakes (M_L = local magnitude) that occurred in the Taipei Metropolitan Area (TMA) from 1973 - 2013 are selected to study the dominant seismicity period of this area. The epicentral distribution and temporal sequences of earthquake magnitudes are simply described. These earthquakes can be divided into two groups: one for events shallower than 40 km and one for events deeper than 60 km. Shallow earthquakes are located mainly in the 0 - 10 km depth range north of 25.1°N, and down to 35 km for those south of 25.1°N. Deep events are located in the subduction zone, with a dip angle of about 70°. The Morlet wavelet technique is applied to analyze the dominant periods of temporal variations in numbers of monthly earthquakes in the shallow and deep ranges for three magnitude ranges, i.e., $M_L \geq 3$, 4, and 5. The results show that for shallow earthquakes the dominant periods are 15.4, 30.8, 66.1, and 132.2 months when $M_L \geq 3$ and 30.8 months when $M_L \geq 4$; while for deep earthquakes, the dominant periods are 16.5 and 141.7 months when $M_L \geq 3$ and 141.7 months when $M_L \geq 4$. The dominant period cannot be obtained for both shallow and deep $M_L \geq 5$ earthquakes.

Key words: Seismicity, Number of monthly events, Morlet wavelet analysis, Wavelet power spectrum, Global power spectrum, Dominant period

Citation: Chen, K. C., J. H. Wang, K. H. Kim, W. G. Huang, K. H. Chang, J. C. Wang, and P. L. Leu, 2015: Morlet wavelet analysis of $M_L \geq 3$ earthquakes in the Taipei Metropolitan Area. Terr. Atmos. Ocean. Sci., 26, 83-94, doi: 10.3319/TAO.2014.09.09.01(T)

1. INTRODUCTION

Taiwan is situated along the collision boundary between the Philippine Sea plate and the Eurasian plate (Tsai et al. 1977; Wu 1978; Lin 2002). The former moves northwestward with a converging speed about 8 cm year^{-1} (Yu et al. 1997). The Philippine Sea plate has subducted underneath the Eurasian plate in northern Taiwan, where the Taipei Metropolitan Area (TMA) (see Fig. 1) is located. This collision causes high seismicity in the Taiwan region (Wang et al. 1983; Wang 1998; Wang and Shin 1998). The TMA is the political, economic and cultural center of Taiwan. Hence, seismic hazard mitigation around the TMA has drawn a lot of attention. For this reason, in-depth investigation of seismicity in the TMA is a high priority. Detailed descriptions of the TMA geology can be found in several previously published articles (e.g., Wang and Lin 1987; Chang et al. 1998; Teng et al. 2001; Wang et al. 2006) and will not be given here.

From 1972 - 1991 the Taiwan Telemetered Seismographic Network (TTSN), sponsored by the National Science Council (NSC), was operated by the Institute of Earth Sciences (IES), Academia Sinica to monitor earthquakes in Taiwan. This network consists of 24 stations, each equipped with a vertical high-gain analog velocity seismometer. Duration magnitude was used by the TTSN to determine the magnitude of earthquakes. Wang (1989a) described this network in detail. Since 1991 the Central Weather Bureau (CWB) has upgraded the old seismic network by adding many new stations. This new network is named the CWB Seismic Network (CWBSN). In 1992 the TTSN was merged

* *Corresponding author*
E-mail: chenkc@earth.sinica.edu.tw

into the CWBSN. The earthquake magnitude catalogue has been unified into the local magnitude. A detailed description of the CWBSN can be found in Shin (1992) and Shin and Chang (2005). At present the CWBSN is composed of 72 stations, each equipped with three-component digital velocity seismometers. Seismograms are recorded in both high- and low-gain forms. This network provides high-quality digital earthquake data to the seismological community.

Although seismicity in the TMA is relatively lower than other areas in Taiwan, numerous earthquakes have occurred in or near the TMA (Hsu 1961, 1971; Wang 1998; Wang et al. 2006; Chen et al. 2010, 2014). During the Emperor Kanshi period of the Chin Dynasty, an event might have occurred in this area in April or May 1694, resulting in an earthquake-induced lake and the destruction of aboriginal houses (Hsu 1983a, b). From historical documents describing the damage, the magnitude of this event was estimated to be 7 by Hsu (1983b) and Tsai (1985). A detailed description concerning historical earthquakes can be found in Wang et al. (2006, 2012a, b, 2014). On 15 April 1909, an M 7.3 earthquake took place at 80-km depth beneath the area, causing 9 deaths, 51 injuries, 122 collapsed houses, and 1054 damaged houses (Hsu 1961). Lin (2005) stressed that seismicity underneath the Taipei Basin, which was usually low, began to increase slightly during the construction period but rose sharply upon the completion of Taipei 101. Three felt earthquakes astonishingly occurred beneath the completed building. Of course, there are debates about induced earthquakes from the load of this building. From the seismicity pattern and focal mechanisms of the three felt events, Chen et al. (2010) suggested the existence of a blind normal fault, whose surface projection is along the river channel in the middle of the basin.

A few previous studies for the seismicity beneath the TMA (e.g., Tsai et al. 1977; Wu 1978; Wang et al. 1983; Wang and Shin 1998; Lin 2002; Wang et al. 2006, 2012a, b, 2014) revealed that there are shallow (0 - 40 km) earthquakes in the crust and deep (> 60 km) ones in the Wadati-Benioff subduction zone. Tsai et al. (1974) found that micro-earthquakes occurred mainly in the southern zone of the Tatun Volcano Group (TVG) where the larger events showed typically normal faulting. The epicentral distributions given by Wang et al. (1983) and Kim et al. (2005) both show lower seismcity in the TMA than other areas in northern Taiwan. Wang (1988) evaluated a higher *b*-value in northern Taiwan than in others. Kim et al. (2005) also obtained a high *b*-value in the TVG. Wang et al. (1994) observed that except for the earthquakes in the subduction zone, the events occurring in northern Taiwan are usually shallow. Kim et al. (2005) also obtained similar results for $M > 2$ events occurred during 1973 - 2003. They also found three $M \geq 2.8$ normal-faulting events below the TVG. Chen and Yeh (1991) observed that most of micro-earthquakes ($0.2 \leq M < 3.0$) in the TVG were located at depths shallower than 10 km and showed normal faulting. Lin et al. (2005) found that the earthquakes underneath the TVG are located mainly at the 2 - 4 km depth range. Konstantinou et al. (2007) observed that all $M < 2.8$ events have a focal depth less than 6 km. Hence, in the TVG high *b*-value, shallow focal depth, and normal faulting may suggest high-temperature related volcanic activities. Based on the concept proposed by Scholz (1990), these studies imply that the seismogenic zone below the TVG would

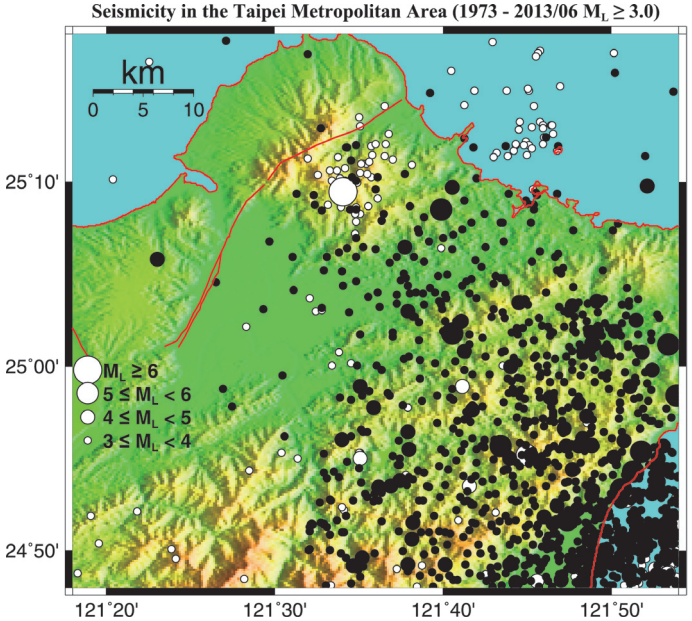

Fig. 1. Epicenters of $M \geq 3$ earthquakes: open and solid circles for shallow (0 - 40 km) and deep (60 - 190 km) events, respectively. Different sized circles show the earthquake magnitudes.

be thinner than that in the other areas. Wang et al. (2006) investigated the epicentral distribution, depth distribution, and temporal sequences of M ≥ 4 earthquakes occurred during 1973 - 2005. Shallow earthquakes in depth range from 0 - 10 km are mainly located north of 25.1°N, and other events down to 35 km in depth are located south of 25.1°N. After 1988, only a few M ≥ 4 shallow events were located in this area. Deep events occurred temporally more or less uniformly during the study time period. The total number of shallow earthquakes decreased annually with time from 1973 - 1988, and varied yearly for deep events. They also applied the FR/QP transition model (cf. Scholz 1990) to interpret the depth distribution of shallow earthquakes.

Seismic risk mitigation knowledge learned from the TMA can be applied to other urban areas in Taiwan and also other seismically active regions around the world. However, previous studies on TMA seismicity are not sufficient for the purpose of mitigating seismic risks. Thus, more comprehensive TMA seismicity studies must be done. One of the most significant studies is exploration of the dominant periods in an earthquake time sequence. Although Fourier analysis is commonly applied to evaluate the dominant periods (or frequency) of a time series, it cannot provide the temporal variations in the dominant periods. The wavelet transform, however, can be used to analyze time series that contain non-stationary power at many different frequencies (Daubechies 1990). In this study wavelet analysis (Combes et al. 1989; Pyrak-Nolte and Nolte 1995), also known as multi-resolution analysis, is taken into account. For this technique a series of scaled and delayed oscillatory functions are used to decompose a time-varying signal into its non-stationary spectral components. Hence, the key advantage of wavelet analysis over traditional Fourier analysis is that the wavelet analysis provides information on how the spectral content varies with time delay. Wavelets are also advantageous over so-called windowed Fourier methods because with wavelets the relative accuracy of the delay and frequency remain constants cover all of the delay-frequency parameter space. Wavelet analysis application to geophysical problems can be seen in Torrence and Compo (1998). Here, a non-orthonormal Morlet wavelet analysis (Morlet et al. 1982) was considered.

This work will focus on evaluating the dominant temporal variation periods in numbers of monthly earthquakes at two depth ranges (the shallow events with focal depths < 40 km and deep ones with focal depths > 60 km) for three magnitude ranges, i.e., M ≥ 3, 4, and 5, occurred in the TMA from 1 January 1973 to 30 June 2013.

2. DATA

From shallow earthquakes occurring in the TMA from 1973 - 1984, Wang (1988) obtained $b = 1.33 \pm 0.13$ in the magnitude range 1.8 - 3.3. For the eastern part of TMA, Wang (1989b) observed $b = 1.21 \pm 0.01$ for events in the 2.1 - 4.8 magnitude range from 1973 - 1985. From shallow earthquakes occurring in the TVG from 1973 - 1999, Kim et al. (2005) estimated $b = 1.22 \pm 0.05$ for the 2.1 - 3.5 magnitude range. Their results show that the earthquake data should be complete when M > 2 in the study area. However, only M ≥ 3 earthquakes occurring in the area (from 121.3 - 121.9°E and 24.8 - 25.3°N) from 1 January 1973 to 30 June 2013 are taken into account for the following reasons: (1) the ability of detecting earthquakes with M < 3 is lower for deep events than shallow ones; and (2) based on seismic risk mitigation, M ≥ 3 earthquakes must be more significant than M < 3 events, because damage caused by M < 3 events is usually very rare.

The earthquake data were retrieved directly from the CWB's data base. The duration magnitude, M_D, was used before 1991; since then the local magnitude, M_L, has been used. It is necessary to have a unified magnitude scale for the two time periods. The maximum location uncertainties are about 2 km horizontally and 5 km vertically from ERH and ERZ of hypo output. The location uncertainty essentially increases with depth. Shin (1993) constructed a conversion formula between M_L and M_D: $M_L = 1.12M_D + 0.03 \pm 0.12$. We converted M_D to M_L for pre-1991 events based on this formula. Hence, a total of 1165 events with magnitude from 3.0 - 6.0 and depth from 0 - 207 km occurred in the TMA from 1 January 1973 to 30 June 2013.

2.1 Spatial Distributions of Earthquakes

The epicenters of the selected earthquakes are plotted in Fig. 1: open circles are shown for shallow (0 - 40 km) earthquakes and solid circles for deep (> 60 km) events as defined by Wang et al. (2006). Because the location uncertainty is smaller than 5 km, the existence of the two groups of events is reliable. Figure 1 shows that deeper earthquakes are located mainly to the east of 121°30'E as pointed out by Tsai et al. (1977), who assumed that the longitude of 120°30'E is the western edge of the northwest dipping subduction zone. Shallow earthquakes have focal depths mainly in the 0 - 10 km range north of 25.1°N and down to 40 km south of 25.1°N. Wang (1989b) and Wang et al. (2006, 2012a, b, 2014) also found that in the eastern part of the TMA the earthquakes are located down to a depth of 40 km. The shallow events to the north of 25.1°N are located mainly at the TVG. Wang et al. (1994, 2006) observed that except for the earthquakes in the subduction zone, the events occurring in northern Taiwan are usually shallow. Kim et al. (2005) also obtained similar results.

2.2 Depth Frequency of Earthquakes

Figure 2 shows the depth distribution of a number of events in a 5-km range along a selected longitude, because

the focal depth error is up to 5 km. These events are divided into two groups. The upper group is in the crust with the largest magnitude of 6.0 occurred on 3 July 1988 and the lower one in the Wadati-Benioff subduction zone. The number of events is much larger for deep earthquakes than for shallow ones. The focal depths of deep events increase from south to north, as they are located in the subduction zone, whose dip angle is about 70° to the north from the pattern of events. Wang and Shin (1998) observed that the subduction zone has an average dip angle of 57° above 120 km and 72° below. Therefore, the subduction zone is concave downward. Since the events in use were located only in a section of the subduction zone just underneath the TMA, such a phenomenon is not displayed here. The number of shallow earthquakes has a peak in the depth ranges from 0 - 5 km and then decreases with depth, while there are several peaks, with the largest one in the depth ranges from 85 - 90 km, around for deep events. The physics that cause the depth distribution frequency of earthquakes can be found in Wang et al. (2006).

2.3 Temporal Variation in Earthquake Magnitudes

Figure 3 shows the earthquake magnitude time series: (a) for shallow and (b) for deep events. The shortest inter-occurrence times are less than 1 day for both shallow and deep earthquakes; while the longest inter-occurrence times are 922.4 and 183.7 days, respectively, for shallow and deep events. It is obvious that after 1988 only three M > 4 shallow events were located in the TMA. Deep events occurred more or less uniformly in the entire study time period. The two time sequences, especially for shallow events, are somewhat different from those in Wang et al. (2012a, b, 2014). The main difference is the fact that the frequency before 1986 was lower in this study than theirs. This is due to the use of different M_D and M_L conversion formulae between this study and theirs. They used the conversion formula made by Yeh and Hsu (1985), which will over-estimate M_L

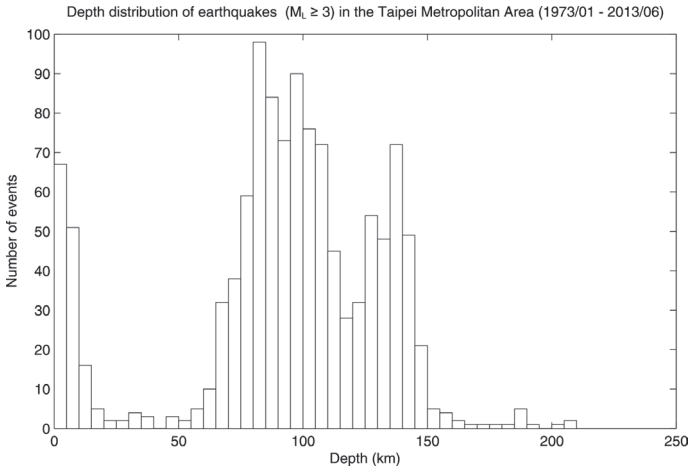

Fig. 2. The depth distribution of the number of events at a depth unit of 5 km.

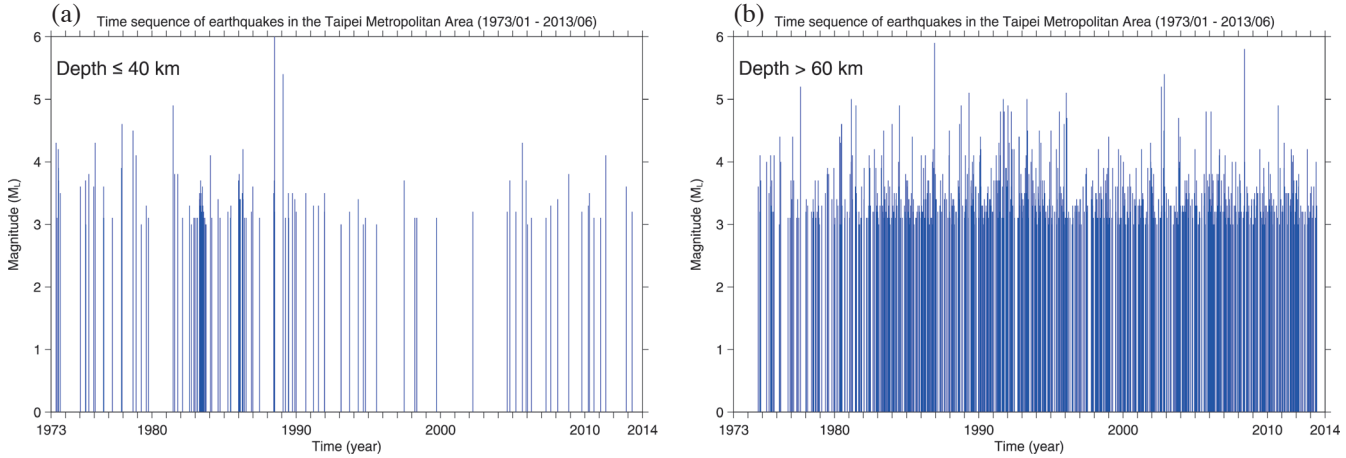

Fig. 3. Time sequences for M ≥ 3 magnitude earthquakes: (a) for shallow events and (b) for deep ones.

from M_D for small events. Hence, there were more events with $M_L \geq 3$ in their studies.

3. MORLET WAVELET ANALYSIS

Assume that there is a time series, x_i, with an equal time spacing δt and $n = 0, \ldots, N - 1$ and $\psi(t)$ is a wavelet function of time t. To be "admissible" as a wavelet, $\psi(t)$ must have zero mean and be localized in both time and frequency space (Farge 1992). An example is the Morlet wavelet, named after Jean Morlet, originally formulated by Goupillaud, Grossmann and Morlet in 1984 (Goupillaud et al. 1984). The main function g(t) is composed of a harmonic wave as a constant k_c subtracted from a plane wave, modulated by a Gaussian envelope. A detailed description of this technique can be found in Torrence and Compo (1998).

The wavelet is written as:

$$\psi(t) = A_c \pi^{-1/4} \exp(-t^2/2)[\exp(i\omega t) - k_c] \quad (1)$$

where $A_c = [1 + \exp(-\omega^2) - 2\exp(-3\omega^2/4)]^{1/2}$ and $k_c = \exp(-\omega^2/2)$. The parameter "ω" in the equation has a dimension of frequency (in Hz or sec^{-1}). Pyrak-Nolte and Nolte (1995) reported $\omega = 2\pi/T_0$ where T_0 is the (characteristic) period of oscillations. In order to avoid some problems caused by small ω, $\omega > 5$ is usually taken into account. Farge (1992) took ω to be 6 to satisfy the admissibility condition. As $\omega = 6$, $T_0 = \sim 1$ sec. As $\omega >> 1$, Eq. (1) can be written as

$$\psi(t) = A_c \pi^{-1/4} \exp(-t^2/2)\exp(i\omega t) \quad (2)$$

The continuous wavelet transform of a discrete sequence x_i is defined as the convolution of x_i with a scaled and translated version of $\psi(t)$:

$$W_n(s) = \Sigma_i x_i \psi^*[(i-n)\delta t/s] \ (i = 0, \ldots, N - 1) \quad (3)$$

where the (*) indicates the complex conjugate, δt is the time shift, and s is the wavelet scale. By varying the wavelet scale s and translating along the localized time index n, a picture can be constructed to show both the amplitude of any features versus the scale and how this amplitude varies with time. Although it is possible to calculate the wavelet transform using Eq. (3), it is considerably faster to perform the calculations in Fourier space.

Because the wavelet function $\psi(t)$ is usually complex the wavelet transform $W_n(s)$ is also complex. The transform can then be divided into the real part $R[W_n(s)]$ and the imaginary part $I[W_n(s)]$. Hence, the amplitude and phase are, respectively, $|W_n(s)|$ and $\theta = \tan^{-1}\{R[W_n(s)]/I[W_n(s)]\}$. Finally, one can define the wavelet power spectrum as $|W_n(s)|^2$.
Let the discrete Fourier transform (DFT) of x_i be χ_i:

$$\chi_k = \Sigma_i x_i e^{-2\pi kn/N} \ (i = 0, \ldots, N - 1) \quad (4)$$

In the continuous limit the Fourier transform of a function $\psi(t/s)$ is given by $F[\psi(s\omega)]$. Using the convolution theorem the wavelet transform is the inverse Fourier transform of the product:

$$W_n(s) = \Sigma_k \chi_k F[\psi \times (s\omega_k)]\exp(i\omega_k n\delta t) \ (k = 0, \ldots, N - 1) \quad (5)$$

To ensure that the wavelet transforms, i.e., Eq, (5), at each scale s are directly comparable to each other and to the transforms of other time series, the wavelet function at each scale s is normalized to have unit energy:

$$F[\psi_o(s\omega_k)] = (2\pi s/\delta t)^{1/2} F[\psi(s\omega_k)] \quad (6)$$

where $\int |F[\psi_o(\omega)]|^2 d\omega = 1$, that is, the function has been normalized to have unit energy.

Using the normalization in Eq. (6) and referring to Eq. (5), the expectation value for $|W_n(s)|^2$ is equal to N times the expectation value for $|\chi_k|^2$. For a white-noise time series this expectation value is σ^2/N, where σ^2 is the variance. Thus, for a white-noise process the expectation value for the wavelet transform is $|W_n(s)|^2 = \sigma^2$ at all n and s.

It is necessary to explain the significance levels of the calculated values. The null hypothesis is defined as follows: it is assumed that the time series has a mean power spectrum; when a peak in the wavelet power spectrum is significantly above this background spectrum, then it can be considered to be a true feature with a certain percentage of confidence. The 95% confidence level implies a test against a certain background level, while the 95% confidence interval refers to the range of confidence about a given value. The normalized Fourier power spectrum is given by $N|\chi_k|^2/2\sigma^2$, where N is the number of data points, χ_k is from Eq. (4), and σ^2 is the variance of the time series.

If x_n is a normally distributed random variable, then both the real and imaginary parts of χ_k are normally distributed (Chatfield 1989). Since the square of a normally distributed variable is chi-square distributed with one degree of freedom (DOF), then $|\chi_k|^2$ is chi-square distributed with two DOFs, denoted by χ_2^2 (Jenkins and Watts 1968). To determine the 95% confidence level (significant at 5%), one multiplies the background spectrum by the 95th percentile value for χ_2^2 (Gilman et al. 1963). The 95% Fourier confidence spectrum will be displayed by a dashed curve below. Note that only a few periods will have power above the 95% line.

In order to meet the equal time interval requirement we consider the number of events occurring in a month to represent the degree of earthquake occurrences. Hence, the dominant periods of time sequence of number of monthly events are evaluated using the Morlet wavelet analysis in the following.

4. RESULTS

The results are displayed in Figs. 4 - 9: Fig. 4 for $M_L \geq 3$ shallow events; Fig. 5 for $M_L \geq 3$ deep events; Fig. 6 for $M_L \geq 4$ shallow events; Fig. 7 for $M_L \geq 4$ deep events; Fig. 8 for $M_L \geq 5$ shallow events; and Fig. 9 for $M_L \geq 5$ deep events. Each figure consists of three panels: (a) for the time sequence of number of monthly events; (b) for the wavelet power spectrum; and (c) for the global wavelet spectrum. In panel (b) the logarithmic values of wavelet power spectrum for different periods (in month) at a certain time span are displayed using distinct colors (from dark red to dark blue). The thick contour is the 95% confidence level using a white-noise background spectrum. The black net region is the cone of influence, where zero padding has reduced the variance. The wavelet power spectrum values inside the net have high uncertainties and thus cannot be taken into account. In each panel (b), the local maximums and local minimums are colored, respectively, by dark red and dark blue. The period related to the local maximum is the local dominant period in a time span. In order to examine the dominant local maximum and related dominant period it is necessary to calculate the average wavelet power spectra from panel (b) over time at a certain period. This average is named the global wavelet spectrum. The results are demonstrated in panel (c), where the solid line represents the global wavelet spectrum and the dashed line denotes the 95% confidence level using a white-noise background spectrum.

Figure 4a shows the time sequence for the number of monthly events for $M_L \geq 3$ shallow earthquakes. There were several large spikes in the time period before 1990. This means that seismicity was higher before 1990 than after 1990 as mentioned previously. Figure 5a shows the time sequence for the number of monthly events for $M_L \geq 3$ deep earthquakes. Except for a spike in 1978, the monthly frequency was lower before 1980 than after 1980. This might be due to a smaller number of seismic stations in those times and thus a lower ability to detect small events, especially for deep ones, before 1980 than after 1980 (see Wang 1989a). After 1980 the seismicity was, on average, uniform, even though the monthly frequency varied with time.

Figures 4b and 5b show the power of the wavelet transform for the monthly events for shallow and deep earthquakes, respectively. The local maximums at several periods in different time spans can be seen. In Figs. 4c and 5c, at certain periods the solid line is close to and to the right of the dashed line. This means that the global wavelet spectrum in this range is significant. At low periods, the global wavelet spectrum peak value is lower than 95% confidence level and thus not taken to be the dominant period. The solid

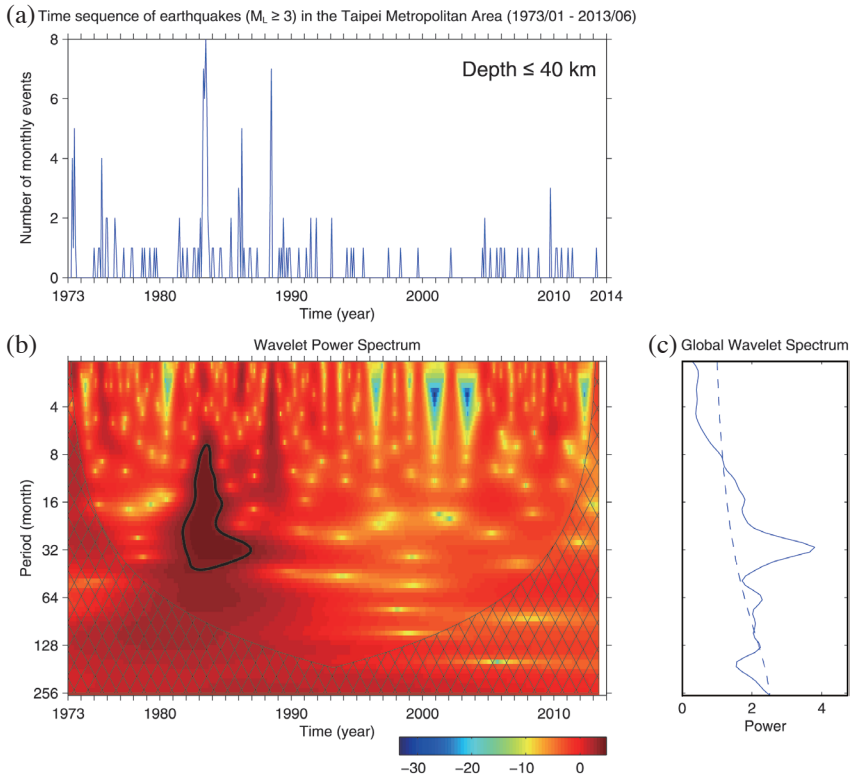

Fig. 4. (a) Time sequence for the number of monthly shallow events with $M_L \geq 3$; (b) for wavelet power spectrum. The thick contour is the 95% confidence level, using a white-noise background spectrum. The black net is described in the text; and (c) for the average, or the global wavelet spectrum, of (b) over all longitudes. The dashed line is the 95% confidence level for the global wavelet spectrum, using a white-noise background spectrum.

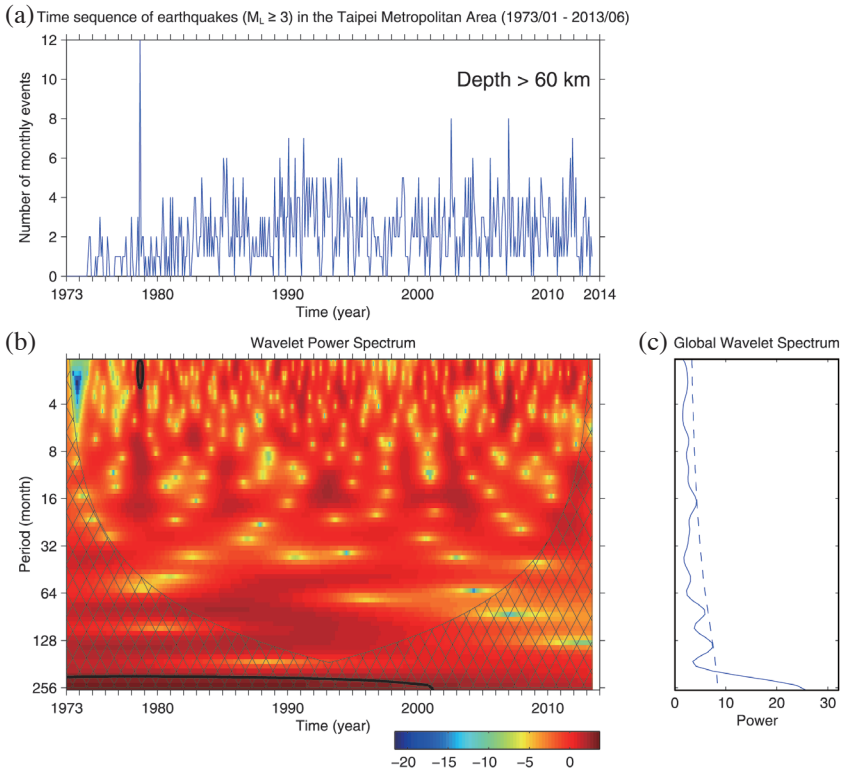

Fig. 5. (a) Time sequence for the number of monthly deep events with $M_L \geq 3$; (b) for wavelet power spectrum. The thick contour is the 95% confidence level, using a white-noise background spectrum. The black net is described in the text; and (c) for the average, or the global wavelet spectrum, of (b) over all longitudes. The dashed line is the 95% confidence level for the global wavelet spectrum, using a white-noise background spectrum.

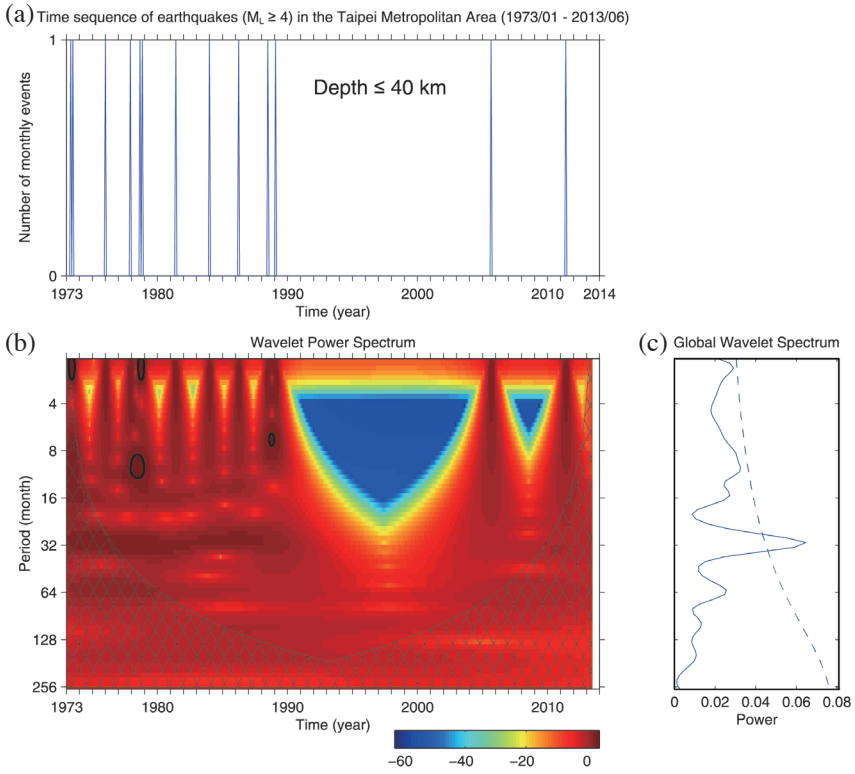

Fig. 6. (a) Time sequence for the number of monthly shallow events with $M_L \geq 43$; (b) for wavelet power spectrum. The thick contour is the 95% confidence level, using a white-noise background spectrum. The black net is described in the text; and (c) for the average, or the global wavelet spectrum, of (b) over all longitudes. The dashed line is the 95% confidence level for the global wavelet spectrum, using a white-noise background spectrum.

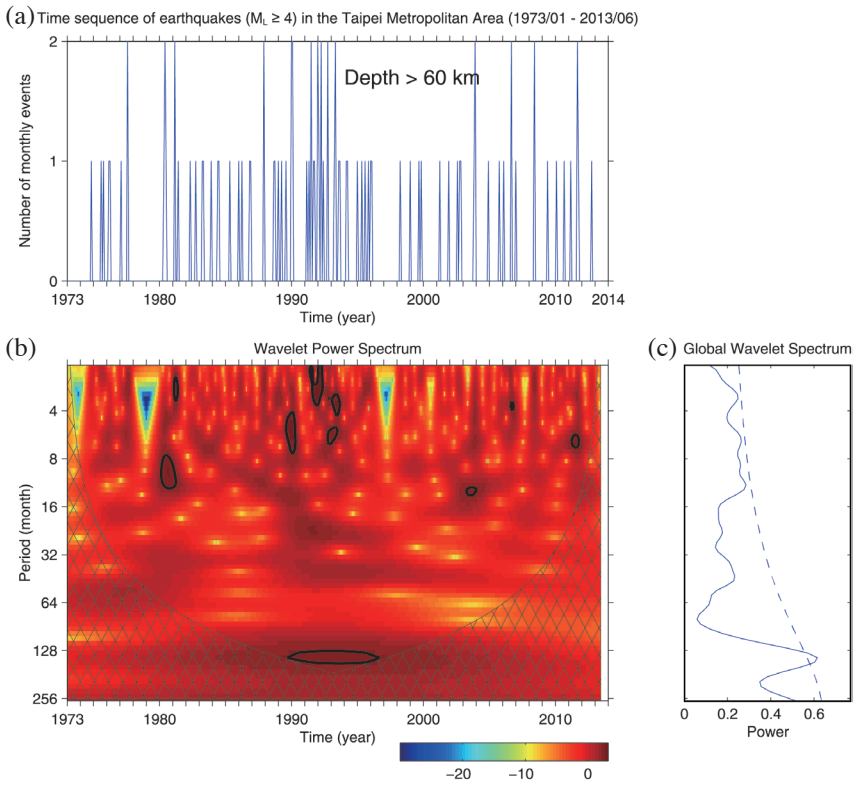

Fig. 7. (a) Time sequence for the number of monthly deep events with $M_L \geq 4$; (b) for wavelet power spectrum. The thick contour is the 95% confidence level, using a white-noise background spectrum. The black net is described in the text; and (c) for the average, or the global wavelet spectrum, of (b) over all longitudes. The dashed line is the 95% confidence level for the global wavelet spectrum, using a white-noise background spectrum.

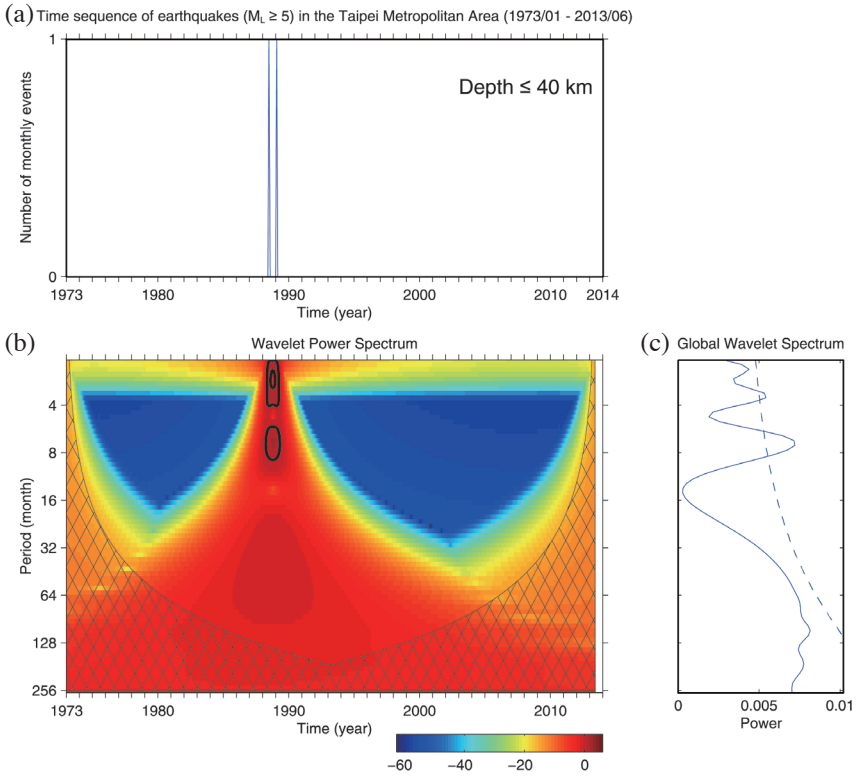

Fig. 8. (a) Time sequence for the number of monthly shallow events with $M_L \geq 5$; (b) for wavelet power spectrum. The thick contour is the 95% confidence level, using a white-noise background spectrum. The black net is described in the text; and (c) for the average, or the global wavelet spectrum, of (b) over all longitudes. The dashed line is the 95% confidence level for the global wavelet spectrum, using a white-noise background spectrum.

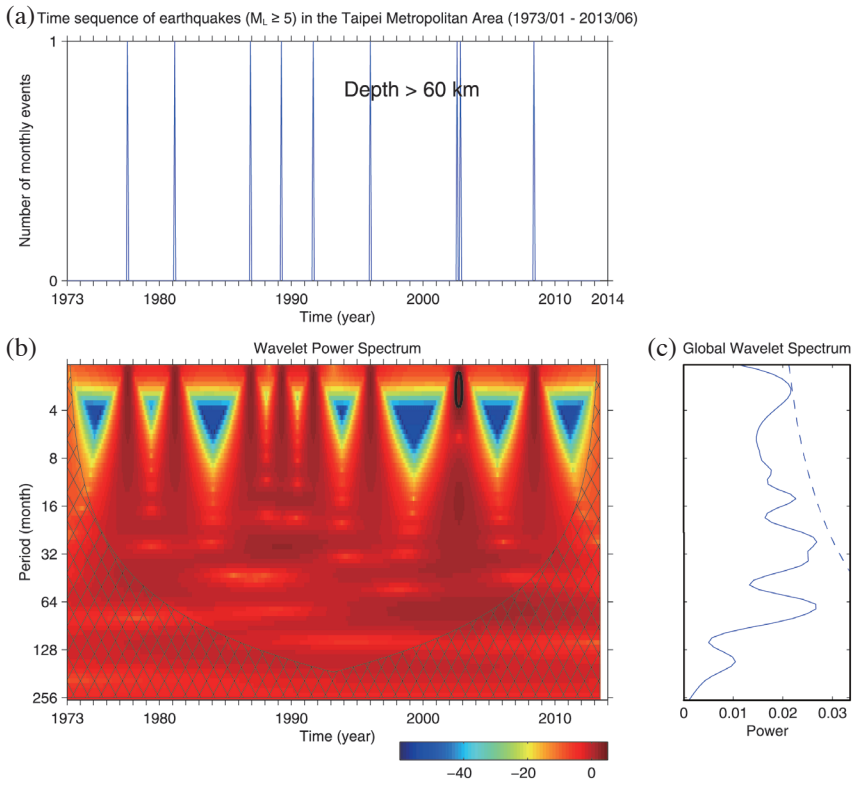

Fig. 9. (a) Time sequence for the number of monthly shallow events with $M_L \geq 5$; (b) for wavelet power spectrum. The thick contour is the 95% confidence level, using a white-noise background spectrum. The black net is described in the text; and (c) for the average, or the global wavelet spectrum, of (b) over all longitudes. The dashed line is the 95% confidence level for the global wavelet spectrum, using a white-noise background spectrum.

line is then close to and to the right of the dashed line. The global wavelet spectrum values abruptly increase at large periods around 32 months in Fig. 4c and around 256 months in Fig. 5c. The solid line is to the right of the dashed line in a large range of periods. Four relative maximum peaks above the 95% confidence level can be observed at 15.4, 30.8, 66.1, and 132.2 months in Fig. 4c and three relative maximum peaks at 16.5, 141.7, and 264.5 months in Fig. 5c. In Fig. 5c, a global wavelet spectrum peak at 264.5 months cannot be considered to be the dominant period because the spectra are inside the "black net."

Figure 6a shows the time sequence of number of monthly events for $M_L \geq 4$ shallow earthquakes. The monthly frequency varied between 0 - 1. The number of line segments was larger before 1990 than after 1990. This means that seismicity was higher before 1990 than after 1990 as mentioned previously. Figure 7a shows the time sequence for the number of monthly events for $M_L \geq 4$ deep earthquakes. Statistically, the monthly frequency was more or less uniform in the whole study period.

Figures 6b and 7b show the local maximums at several periods in different time spans. Figure 6c shows that although at two low periods the solid line is close to the dashed line, it is still to the left of the dashed line. This means that the global wavelet spectra at the two periods are less significant. When at the period of 30.8 months, the peak global wavelet spectrum value is higher than 95% confidence level and thus this period is taken to be the dominant period. Figure 7c shows that although at a few low periods the solid line is close to the dashed line, it is still to the left of the dashed line. This means that the global wavelet spectra at those periods are less significant. When at the 141.7 month period the peak value of the global wavelet spectrum is higher than 95% confidence level and thus this period taken to be the dominant period.

Figure 8a shows the time sequence of number of monthly events for $M_L \geq 5$ shallow earthquakes. Essentially, there were only two spikes in the time interval from 1988 - 1990. Hence, the wavelet power spectra of the time sequence as shown in Fig. 8b is quite abnormal. Although at two periods (3.6 and 7.2 months) in Fig. 8c the solid line is to the right of the dashed line, the two periods cannot be considered to be the dominant periods because of a small number of data of the time sequence in a very short time span from 1988 - 1990.

Figure 9a shows the time sequence for the number of monthly events for $M_L \geq 5$ deep earthquakes. Obviously, there were several spikes with non-equal time intervals. Figure 9b shows local maximums at several periods in different time spans. Figure 9c shows that in a small range at

low periods around 2.9 months the solid line is very close to but not to the right of the dashed line. This means that the global wavelet spectrum in this period range is not significant. Hence the period of 2.9 months cannot be considered to be the dominant period of the time sequence.

The dominant period is significant when its peak value is higher than the related 95% confidence level. The period associated with such a peak is taken to be the dominant period. The results are given in Table 1 for shallow and deep earthquakes in three different magnitude ranges.

Table 1. The dominant periods (in months) of time sequences of numbers of monthly events for shallow (S) and deep (D) earthquakes in three magnitude ranges: M ≥ 3, 4, and 5.

M ≥ 3		M ≥ 4		M ≥ 5	
S	D	S	D	S	D
15.4	16.5				
30.8		30.8			
66.1	141.7		141.7		
132.2					

5. DISCUSSION AND CONCLUSIONS

The $M_L \geq 3$ earthquakes that occurred below the TMA from 1973 - 2013 can be divided into shallow (< 40 km) and deep (> 60 km) earthquakes, which are located in the crust and subduction zones, respectively. There is an average depth difference of about 20 km between the two groups. The part of the subduction zone related to deep events has a dip angle of about 70°. Shallow earthquakes are located mainly in the 0 - 10 km depth rang north of 25.1°N and down to 40 km south of 25.1°N. On the other hand, deep earthquakes are distributed in a wide range from 60 km to more than 200 km, with the peak frequency in the 85 - 90 km range.

Figures 6a and 7a show that in some time spans few line segments are close to one another. This suggests the possible existence of repeat events within a short time period. However, the amount of time sequence data is not enough to form a complete cycle to provide a significant dominant period.

The dominant periods obtained from Morlet wavelet analysis are listed in Table 1 for shallow and deep earthquakes in three magnitude ranges: $M_L \geq 3$, 4, and 5. Because there are only two data in the time sequence for $M_L \geq 5$, the wavelet power spectrum is too strange to provide significant information to evaluate the dominant period of this sequence. Figure 4c shows that for shallow earthquakes there are peaks in the solid line at four dominant periods, i.e., 15.4, 30.8, 66.1, and 132.2 months. The latter three dominant periods are almost 2, 4, and 9 times the first one. Figure 5c displays that for deep earthquakes there are only two peaks in the solid line at 16.5 and 141.7 months. The related dominant period is longer for deep earthquakes than shallow ones. Figure 6c shows a peak in the solid line at 30.8 months, which is the second dominant period for $M_L \geq 3$ earthquakes. It is obvious from Fig. 6a that the peak period at 30.8 months cannot be considered to be the dominant period for the whole time sequence in the time interval from 1973 - 1990. Figure 7c shows a peak in the solid line at 141.7 months, which is the fourth dominant period for $M_L \geq 3$ earthquakes. The latter is about 9 times the former. Figures 6c and 7c show that at low periods there are a few peaks for shallow earthquakes and two peaks for deep events. The global wavelet spectra are very close to the corresponding dashed lines. Nevertheless, those periods are not taken into account because the global wavelet spectra are still to the left of the corresponding dashed lines.

As mentioned previously the amount of data for $M_L \geq 5$ shallow earthquakes is quite small, as shown in Fig. 8a. The wavelet power spectrum (Fig. 8b) and the global wavelet spectrum (Fig. 8c) are not normal. The dominant period cannot be obtained for $M_L \geq 5$ shallow earthquakes. For $M_L \geq 5$ deep earthquakes the dominant period cannot be obtained because the solid line is to the left of the dashed line, as displayed in Fig. 9b. Hence, we cannot infer the dominant period for both shallow and deep $M_L \geq 5$ earthquakes.

Table 1 shows that for $M_L \geq 3$ time sequences, the dominant period is slightly longer for deep earthquakes than for shallow events. This means that the repeat time for high seismicity shallow earthquakes is slightly shorter than that for deep events. For $M_L \geq 4$ time sequences the dominant period is longer for deep earthquakes than for shallow events. Because the number of events is larger for deep earthquakes than shallow events, the reasons for the previous observation are still open.

Acknowledgements The authors would like to thank the Central Weather Bureau for providing earthquake data. Helpful comments from Jer-Ming Chiu and one anonymous reviewer greatly improved the manuscript. This work was sponsored by Academia Sinica under Grant No. AS-102-SS-A09 and the Ministry of Science and Technology under Grant No. MOST 103-2116-M-001-021 (for K. C. Chen) and Grant No. NSC102-2116-M-001-021 (for J. H. Wang). This work was partially funded by the KMA, Research Development Program under Grant CATER 2014-8020 (for K. H. Kim).

REFERENCES

Chang, H. C., C. W. Lin, M. M. Chen, and S. T. Lu, 1998: An introduction to the active faults of Taiwan. Explanatory Text of the Active Fault Map of Taiwan SCALE 1:55000, Central Geol. Surv., MOEA, ROC, 103 pp. (in Chinese)

Chatfield, C., 1989: The Analysis of Time Series: An

Introduction, 4th edition, Chapman & Hall, New York, 241 pp.

Chen, K. C., B. S. Huang, W. G. Huang, J. H. Wang, K. H. Kim, S. J. Lee, Y. C. Lai, S. Tsao, and C. H. Chen, 2010: A blind normal fault beneath the Taipei basin in northern Taiwan. *Terr. Atmos. Ocean. Sci.*, **21**, 495-502, doi: 10.3319/TAO.2010.01.25.01(TH). [Link]

Chen, K. C., J. H. Wang, K. H. Kim, and P. L. Leu, 2014: Strong ground motions generated by the February 11, 2014 Tatunshan Earthquake in the Taipei Metropolitan Area. *Terr. Atmos. Ocean. Sci.*, **25**, 709-718, doi: 10.3319/TAO.2014.05.27.01(T). [Link]

Chen, K. J. and Y. H. Yeh, 1991: Gravity and microearthquake studies in the Chinshan-Tanshui area, northern Taiwan. *Terr. Atmos. Ocean. Sci.*, **2**, 35-50.

Combes, J. M., A. Grossmann, and P. Tchamitchian, 1989: Wavelets: Time-Frequency Methods and Phase Space, Inverse Problems and Theoretical Imaging, Springer-Verlag Berlin Heidelberg, doi: 10.1007/978-3-642-97177-8. [Link]

Daubechies, I., 1990: The wavelet transform, time-frequency localization and signal analysis. *IEEE T. Inform. Theory*, **36**, 961-1005, doi: 10.1109/18.57199. [Link]

Farge, M., 1992: Wavelet transforms and their applications to turbulence. *Annu. Rev. Fluid Mech.*, **24**, 395-457, doi: 10.1146/annurev.fl.24.010192.002143. [Link]

Gilman, D. L., F. J. Fuglister, and J. M. Mitchell Jr., 1963: On the power spectrum of "red noise". *J. Atmos. Sci.*, **20**, 182-184, doi: 10.1175/1520-0469(1963)020<0182:OTPSON>2.0.CO;2. [Link]

Goupillaud, P., A. Grossmann, and J. Morlet, 1984: Cycle-octave and related transforms in seismic signal analysis. *Geoexploration*, **23**, 85-102, doi: 10.1016/0016-7142(84)90025-5. [Link]

Hsu, H., 1983a: Source materials on the history of natural disasters in Ching Taiwan. Hazards Mitigation S&T Report, 72-01, 5-6. (in Chinese)

Hsu, M. T., 1961: Seismicity of Taiwan (Formosa). *Bull. Earthq. Res. Inst.*, **39**, 831-847.

Hsu, M. T., 1971: Seismicity of Taiwan and some related problems. *Bull. Int. Inst. Seism. Earthquake Engin., Japan*, **8**, 41-160.

Hsu, M. T., 1983b: Estimation of earthquake magnitudes and seismic intensities of destructive earthquakes in the Ming and Ching Eras. *Meteorol. Bull.*, **29**, 1-18. (in Chinese)

Jenkins, G. M. and D. G. Watts, 1968: Spectral Analysis and Its Applications, Holden-Day, San Francisco, 525 pp.

Kim, K. H., C. H. Chang, K. F. Ma, J. M. Chiu, and K. C. Chen, 2005: Modern seismic observations in the Tatun volcano region of northern Taiwan: Seismic/volcanic hazard adjacent to the Taipei Metropolitan area. *Terr. Atmos. Ocean. Sci.*, **16**, 579-594.

Konstantinou, K. I., C. H. Lin, and W. T. Liang, 2007: Seismicity characteristics of a potentially active Quaternary volcano: The Tatun Volcano Group, northern Taiwan. *J. Volcanol. Geotherm. Res.*, **160**, 300-318, doi: 10.1016/j.jvolgeores.2006.09.009. [Link]

Lin, C. H., 2002: Active continental subduction and crustal exhumation: The Taiwan orogeny. *Terr. Nova*, **14**, 281-287, doi: 10.1046/j.1365-3121.2002.00421.x. [Link]

Lin, C. H., 2005: Seismicity increase after the construction of the world's tallest building: An active blind fault beneath the Taipei 101. *Geophys. Res. Lett.*, **32**, L22313, doi: 10.1029/2005GL024223. [Link]

Lin, C. H., K. I. Konstantinou, W. T. Liang, H. C. Pu, Y. M. Lin, S. H. You, and Y. P. Huang, 2005: Preliminary analysis of volcanoseismic signals recorded at the Tatun Volcano Group, northern Taiwan. *Geophys. Res. Lett.*, **32**, L10313, doi: 10.1029/2005GL022861. [Link]

Morlet, J., G. Arens, E. Fourgeau, and D. Giard, 1982: Wave propagation and sampling theory-Part II: Sampling theory and complex waves. *Geophysics*, **47**, 222-236, doi: 10.1190/1.1441329. [Link]

Pyrak-Nolte, L. J. and D. D. Nolte, 1995: Wavelet analysis of velocity dispersion of elastic interface waves propagating along a fracture. *Geophys. Res. Lett.*, **22**, 1329-1332, doi: 10.1029/95GL01323. [Link]

Scholz, C. H., 1990: The Mechanics of Earthquakes and Faulting, Cambridge University Press, New York, 439 pp.

Shin, T. C., 1992: Some implications of Taiwan tectonic features from the data collected by the Central Weather Bureau Seismic Network. *Meteorol. Bull.*, **38**, 23-48. (in Chinese)

Shin, T. C., 1993: The calculation of local magnitude from the simulated Wood-Anderson seismograms of the short-period seismograms in the Taiwan area. *Terr. Atmos. Ocean. Sci.*, **4**, 155-170.

Shin, T. C. and J. S. Chang, 2005: Earthquake monitoring systems in Taiwan. In: Wang, J. H., C. Y. Wang, Q. C. Sung, T. C. Shin, S. B. Yu, C. F. Shieh, K. L. Wen, S. L. Chung, M. Lee, K. W. Kuo, and K. C. Chang (Eds.), The 921 Chi-Chi Major Earthquake, Office of Inter-Ministry S&T Program for Earthquake and Active-fault Research, NSC, 43-59. (in Chinese)

Teng, L. S., C. T. Lee, C. H. Peng, W. F. Chen, and C. J. Chu, 2001: Origin and geological evolution of the Taipei Basin, northern Taiwan. *West. Pac. Earth Sci.*, **1**, 115-142.

Torrence, C. and G. P. Compo, 1998: A practical guide to wavelet analysis. *Bull. Amer. Meteorol. Soc.*, **79**, 61-78, doi: 10.1175/1520-0477(1998)079<0061:APGTWA>2.0.CO;2. [Link]

Tsai, Y. B., 1985: A study of disastrous earthquake in Taiwan, 1683-1895. *Bull. Inst. Earth Sci. Acad. Sin.*, **5**, 1-44.

Tsai, Y. B., H. B. Liaw, and C. C. Feng, 1974: A study of microearthquakes in the Tatun volcanic region in

northern Taiwan. *Annu. Rep. Inst. Phys. Acad. Sin.*, 239-250.

Tsai, Y. B., T. L. Teng, J. M. Chiu, and H. L. Liu, 1977: Tectonic implications of the seismicity in the Taiwan region. *Mem. Geol. Soc. China*, **2**, 13-41.

Wang, C. M. and T. P. Lin, 1987: The geology and land subsidence of the Taipei Basin. *Mem. Geol. Soc. China*, **9**, 447-464.

Wang, C. Y. and T. C. Shin, 1998: Illustrating 100 years of Taiwan seismicity. *Terr. Atmos. Ocean. Sci.*, **9**, 589-614.

Wang, J. H., 1988: *b* values of shallow earthquakes in Taiwan. *Bull. Seismol. Soc. Am.*, **78**, 1243-1254.

Wang, J. H., 1989a: The Taiwan Telemetered Seismographic Network. *Phys. Earth Planet. Inter.*, **58**, 9-18, doi: 10.1016/0031-9201(89)90090-3. [Link]

Wang, J. H., 1989b: Aspects of seismicity in the southernmost part of the Okinawa trough. *Proc. Geol. Soc. China*, **32**, 79-99.

Wang, J. H., 1998: Studies of earthquake seismology in Taiwan during the 1897-1996 period. *J. Geol. Soc. China*, **41**, 291-336.

Wang, J. H., Y. B. Tsai, and K. C. Chen, 1983: Some aspects of seismicity in Taiwan region. *Bull. Inst. Earth Sci. Acad. Sin.*, **3**, 87-104.

Wang, J. H., K. C. Chen, and T. Q. Lee, 1994: Depth distribution of shallow earthquakes in Taiwan. *J. Geol. Soc. China*, **37**, 125-142.

Wang, J. H., M. W. Huang, and W. G. Huang, 2006: Aspects of M≥4 earthquakes in the Taipei metropolitan area. *West. Pac. Earth Sci.*, **6**, 169-190.

Wang, J. H., K. C. Chen, S. J. Lee, W. G. Huang, Y. H. Wu, and P. L. Leu, 2012a: The frequency distribution of inter-event times of $M \geq 3$ earthquakes in the Taipei metropolitan area: 1973 - 2010. *Terr. Atmos. Ocean. Sci.*, **23**, 269-281, doi: 10.3319/TAO.2011.12.20.01(T). [Link]

Wang, J. H., K. C. Chen, S. J. Lee, W. G. Huang, and P. L. Leu, 2012b: Fluctuation analyses of M ≥ 3 earthquake sequences in the Taipei Metropolitan Area. *Terr. Atmos. Ocean. Sci.*, **23**, 633-645 doi: 10.3319/TAO.2012.08.14.01(T). [Link]

Wang, J. H., K. C. Chen, W. G. Huang, K. H. Chang, J. C. Wang, and P. L. Leu, 2014: Multifractal measures of M ≥ 3 shallow earthquakes in the Taipei metropolitan area. *Terr. Atmos. Ocean. Sci.*, **25**, 17-26, doi: 10.3319/TAO.2013.09.09.01(T). [Link]

Wu, F. T., 1978: Recent tectonics of Taiwan. *J. Phys. Earth*, **26**, S265-S299.

Yeh, Y. T. and P. S. Hsu, 1985: Catalog of earthquakes in Taiwan from 1644 to 1984, Open-file Report, Institute of Earth Sciences, Academia Sinica, Taipei, Taiwan.

Yu, S. B., H. Y. Chen, and L. C. Kuo, 1997: Velocity field of GPS stations in the Taiwan area. *Tectonophysics*, **274**, 41-59, doi: 10.1016/S0040-1951(96)00297-1. [Link]